Citation for final published version:

Publishers page: http://dx.doi.org/10.1002/aenm.201602328

Chlorine-Enabled Electron Doping in Solution-Synthesised SnSe Thermoelectric Nanomaterials; Supporting Information.

Guang Han,[a] Srinivas R. Popuri,[b] Heather F. Greer,[c] Jan-Willem G. Bos,[b] Wuzong Zhou,[c] Hervé Ménard,[d] Andrew R. Knox,[e] Andrea Montecucco,[e] Jonathan Siviter,[e] Elena A. Man,[e] Wen-guang Li,[e] Manosh C. Paul,[e] Douglas J. Paul,[e] Min Gao,[f] Tracy Sweet,[f] Robert Freer,[g] Feridoon Azough,[g] Hasan Baig,[h] Tapas K. Mallick,[h] and Duncan H. Gregory[a*]

[a]WestCHEM, School of Chemistry, University of Glasgow, Glasgow, G12 8QQ, UK

[b]Institute of Chemical Sciences and Centre for Advanced Energy Storage and Recovery, School of Engineering and Physical Sciences, Heriot-Watt University, Edinburgh, EH14 4AS, UK

[c]EaStCHEM, School of Chemistry, University of St Andrews, St Andrews, Fife KY16 9ST, UK

[d]Sasol (UK) Ltd, St Andrews, KY16 9ST, UK

[e]School of Engineering, University of Glasgow, Glasgow, G12 8QQ, UK

[f]School of Engineering, Cardiff University, Cardiff, CF24 3AA, UK

[g]School of Materials, University of Manchester, Manchester, M13 9PL, UK

[h]Environment and Sustainability Institute, University of Exeter, Penryn Campus, Penryn TR10 9FE UK

*Corresponding author: Email: Duncan.Gregory@glasgow.ac.uk

Experimental details

Materials Synthesis. In a typical synthesis of SnSe nanoparticles, 260 mmol citric acid (Alfa, 99.5%) and 10 mmol $SnCl_2 \cdot 2H_2O$ (Sigma, 99.99%) were added into 50 ml deionised water (DIW) within a two-neck round-bottom flask to yield a transparent solution. In parallel, 10 mmol Se (Aldrich, >99.5%) and 20 mmol $NaBH_4$ (Alfa, 98%) were added to 50 ml DIW within a single-neck round-bottom flask, to prepare a transparent NaHSe solution ($2Se + 4NaBH_4 + 7H_2O \rightarrow 2NaHSe + Na_2B_4O_7 + 14H_2\uparrow$). After the $SnCl_2$-citric acid solution was heated to its boiling temperature using an oil bath, the freshly prepared 50 ml NaHSe aqueous solution was injected into the solution, leading to the immediate formation of a black precipitate. The mixture was heated to boiling again, held for either 1 min, 5 min, 2 h or 24 h and allowed to cool to room temperature under Ar (BOC, 99.998%) on a Schlenk line. The products were collected by centrifuge, washed with DIW and ethanol several times, and dried in ambient atmosphere at 50 ℃ for 12 h. Scaled-up syntheses were performed with 5.5-fold precursor concentrations, i.e. using 1430 mmol citric acid, 55 mmol $SnCl_2 \cdot 2H_2O$, and 275 ml NaHSe solution (0.2 mol L^{-1}); the products demonstrated phase purity and morphology identical to the products synthesised at lower precursor concentrations. For the surfactant-free synthesis of SnSe nanoparticles, 4 ml hydrochloric acid (Sigma, 36.5-38%) was introduced into $SnCl_2$ solution in place of 50 g citric acid, while the other experimental conditions were unchanged. The synthesised samples used for characterisation and performance evaluation were stored in an Ar-filled MBraun glove box (< 0.5 ppm H_2O, < 0.5 ppm O_2) to avoid possible reaction with ambient air.

Materials Characterisation and Performance Evaluation. The phase composition and crystal structures of the as-prepared samples were investigated by powder X-ray diffraction (PXD), using a PANalytical X'pert Pro MPD diffractometer in Bragg-Brentano geometry (Cu Kα1 radiation, λ = 1.5406 Å). Diffraction data were collected at room temperature with a step size of 0.017º over 10º ≤ 2θ ≤ 90º for 1 h (for phase indexing) or over 10º ≤ 2θ ≤ 100º for 8-12 h (for structural refinement).

In-situ variable-temperature PXD measurements were performed on a 2 h solution-synthesised sample that was loaded into a sample holder under ambient atmosphere. The sample was heated to the selected temperatures under a constant Ar flow (BOC, 99.998%) using an Anton Paar HK1200N high-temperature cell with Kapton windows. The sample was progressively heated from room temperature to 700 K in steps of 50 K at a rate of 5 K min^{-1} and the PXD patterns were collected at each temperature with a step size of 0.017° from 10° ≤ 2θ ≤85° over a period of 1 h. The sample was subsequently cooled to 500 K and then 300 K at a rate of ~10 K min^{-1} under Ar flow and PXD data were collected at each temperature. The crystal structures of the synthesised products were refined using the Rietveld method against PXD data with the GSAS and EXPGUI software packages[1] and the previously published SnSe,[2] $SnSe_2$,[3] and SnO_2[4] structures as a basis. For Rietveld refinement against PXD data of pellet samples, a shifted Chebyschev function (type 1 within GSAS) and a Pseudo-Voigt profile function (type 2 within GSAS) were applied to model the background and peak shape respectively, and a March-Dollase preferred orientation parameter along (400) of SnSe and (001) of $SnSe_2$ was introduced and refined.

The morphological and chemical characteristics of the synthesised products were investigated by scanning electron microscopy (SEM, Carl Zeiss Sigma, 5 and 20 kV for imaging and elemental analyses, respectively), equipped with energy-dispersive X-ray spectroscopy (EDS, Oxford Instruments X-Max 80). The synthesised powders were spread on a conductive carbon tape that was then mounted on a standard SEM sample stub. Microstructure and crystal structure were further characterised by transmission electron microscopy (TEM) using an FEI Titan Themis 200 electron microscope equipped with an X-FEG Schottky field emission gun, and a JEOL JEM-2011 electron microscope fitted with a LaB_6 filament, both operating at an accelerating voltage of 200 kV. TEM images, high resolution TEM (HRTEM) images and selected area electron diffraction (SAED) patterns were recorded using an FEI Ceta 16-megapixel CMOS camera (FEI Titan Themis 200) and a Gatan 794 Multiscan CCD camera (JEOL JEM-2011). To prepare TEM samples from SnSe pellets, SnSe powders were peeled from the pellet surface using a blade followed by a gentle crushing using

mortar and pestle. The peeled SnSe powders or solution-synthesised SnSe powders were dispersed in ethanol by sonication for 30 s to obtain a uniform dispersion. 2-5 drops of the suspension were dropped on to a 3 mm diameter holey C-coated Cu TEM grid.

As-synthesised SnSe samples were directly mounted in a Fourier transform infrared (FTIR) spectrophotometer (Shimadzu, FTIR-8400S) to obtain FTIR spectra at room temperature. Thermogravimetric-differential thermal analysis (TG-DTA) of the samples was performed using a Netzsch STA 409 thermal analyser located in an Ar-filled MBraun glove box (< 0.1 ppm H_2O, < 0.1 ppm O_2). Approximately 25 mg of SnSe pellet or powder was heated to 700 °C in an alumina pan under flowing Ar at a heating rate of 5 °C min^{-1}. For optical bandgap measurement, SnSe powders were spread into a thin uniform layer on a layer of $BaSO_4$ powder, and diffuse reflectance UV-Vis (DR-UV-Vis) spectra were measured using a UV-Vis spectrophotometer (Shimadzu, UV-2600) within a wavelength range of 400-1300 nm. The XPS experiments were performed using a Kratos Axis Ultra-DLD photoelectron spectrometer with an Al monochromatic X-ray source. The data were analysed using CasaXPS software.

To measure the electrical performance of SnSe nanostructures, SnSe powder was loaded into a graphite die and hot-pressed into dense pellets (relative density of $> 85\%$) at 500 °C for 20 min under Ar protection with a uniaxial pressure of ~60 MPa. The obtained pellets were cut into bars with dimensions of 12 mm x 3 mm x 2 mm, and the Seebeck coefficient and electrical conductivity of the SnSe bars were measured perpendicular to the hot pressing direction using a Linseis LSR-3 instrument under a helium atmosphere within a temperature range of 300-540 K. The uncertainty in the measurement of the Seebeck coefficient and electrical conductivity is 5%, leading to ~10% uncertainty for the thermoelectric power factor measurement.

Oxidation Experiments

Three experiments were designed and performed in an effort to understand the origins of the oxidation process further. First, we subjected the SnSe nanoparticles (samples prepared for 1 min, 2

h and 24 h) to TG-DTA (Figure S7) (Netzsch STA 409 instrument located in an Ar-filled MBraun glove box with < 0.1 ppm H_2O, < 0.1 ppm O_2). PXD analysis (Figure S8) of the post-TG-DTA samples reveals that a small amount of SnO_2 was produced and this amount increases as the solution reaction duration decreases. Considering that SnSe nanoparticles are apparently coated with higher concentrations of citric acid (Figure S9) at shorter reaction durations and higher weight losses (corresponding to oxidation) were observed for these shorter-duration samples, it is tempting to infer that the carboxylic groups bound to the surface contribute to SnO_2 formation (as indicated by the exothermic DTA peak at ~330 ℃; Figure S7).[5] The excess Se generated from the formation of SnO_2 volatilises as evidenced by the significant weight decrease between 500 and 700 ℃ (Figure S7); therefore, no $SnSe_2$ phase was detected in the PXD patterns of the TG-DTA products as might be expected as a result of equation S1 below:

$$SnSe + O_2 \quad \rightarrow \quad SnO_2 + Se \uparrow \qquad (S1)$$
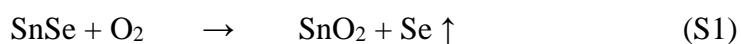
In a second experiment, we prepared SnSe nanoparticles using a similar solution method replacing citric acid with hydrochloric acid in reactions of either 2 h or 24 h duration (Figures S10, S11; Table S4). We hot pressed these surfactant-free nanoparticles into pellets (denoted as **SF1** and **SF2**) and PXD patterns again indicate the presence of SnO_2 and $SnSe_2$ as secondary phases to SnSe (Figure S12, S13; Table S5, S6). This suggests that the surfaces of the small nanoparticles may adsorb O_2 thus leading in turn to oxidation to SnO_2. As hot pressing was performed in enclosed dies, the Se byproduct (following formation of SnO_2) is not released from the system as in the TG-DTA experiment (above) and leads to the formation of the Se-rich phase $SnSe_2$.

Finally, to probe the formation process of $SnSe_2$ and SnO_2 during heating of SnSe nanoparticles, we performed *in-situ* variable temperature PXD experiments with 2 h-synthesised SnSe nanoparticles. The powder was loaded into a PXD holder (under air) and heated under an Ar gas flow so as to simulate the environmental conditions of the hot pressing process applied in this study (Figure S14).

As can be seen, crystalline $SnSe_2$ and SnO_2 start to form at approximately 500 K and 600 K, respectively. The Bragg peak width of SnSe decreased notably by 700 K, indicating the increased particle size. Moreover, it is assumed that sublimation of Se took place at 650-700 K, leading to the decreased relative intensity of $SnSe_2$. Following Se sublimation on cooling, the final products that dominate the diffractogram are principally SnSe and SnO_2 as a minor phase, which is approximately consistent with the PXD analysis of post-TG-DTA products above. Therefore, the experimental evidence would suggest that SnO_2 forms both as a result of desorbing and reacting surface carboxylate groups[5] and from the reaction of the very small, high surface area nanoparticles with adventitious O_2.[6] It should be noted that reports of oxidation also exist for solution-synthesised PbTe nanowires and Bi_2Te_3 nanoparticles that were subsequently pressed at high temperature,[7] and SnO_2 precipitates were observed in SnSe pellets that were consolidated by spark plasma sintering from fine SnSe powders (prepared by mechanical alloying).[6]

Figure S1. Digital photographs showing (a) the nanoparticle solution after a synthesis and (b) a typical yield of SnSe nanoparticles (~10.4 g, *ca*. 96 %) produced in a one-pot synthesis.
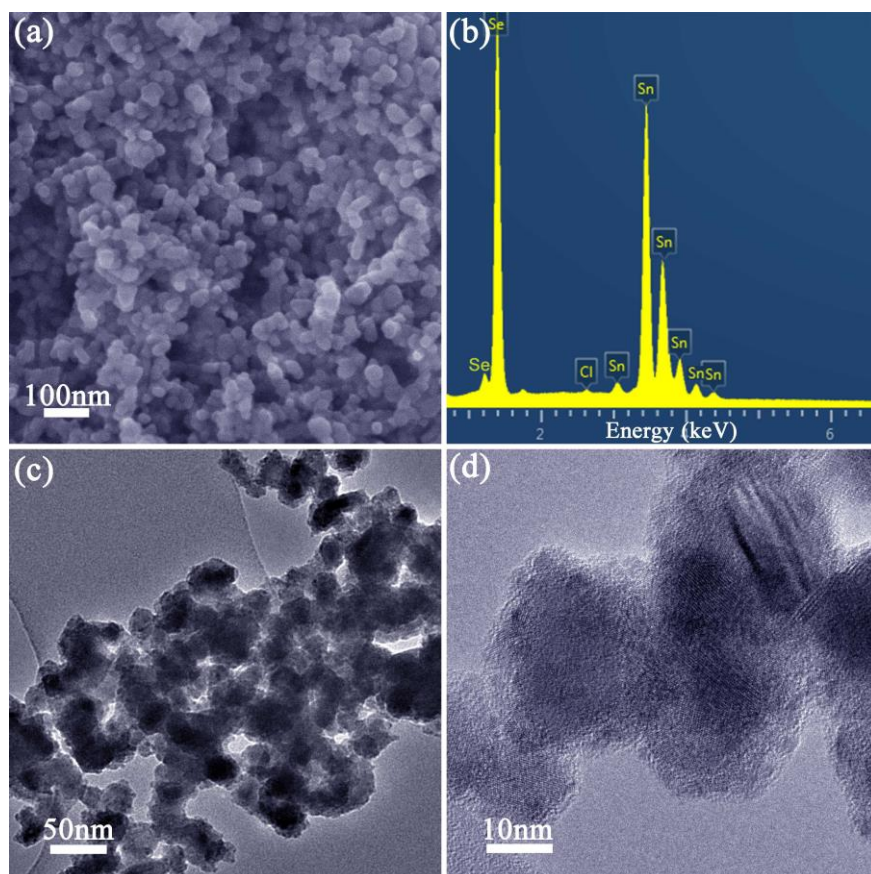

Figure S2. (a) SEM image; (b) EDS spectrum; (c,d) TEM images of SnSe nanoparticles synthesised after 2 h of heating.
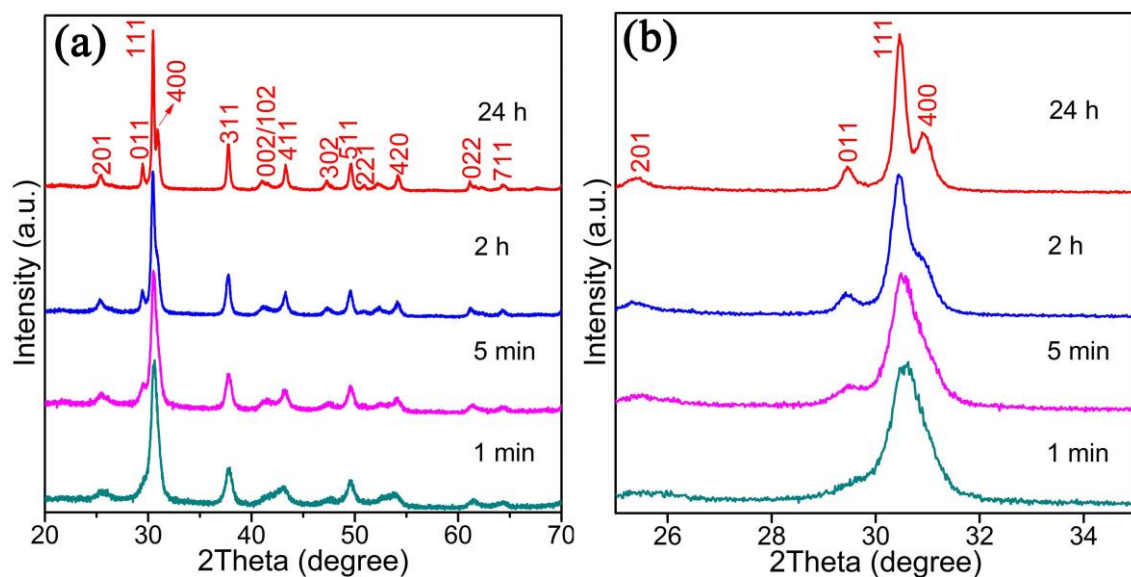
Figure S3. PXD patterns of SnSe nanoparticles synthesised after 1 min, 5 min, 2 h and 24 h of heating respectively, with all reflections indexed to orthorhombic SnSe: (a) scans from $20 \leq 2\theta/° \leq 70$ and (b) detail of the (201), (011), (111) and (400) Bragg peaks.
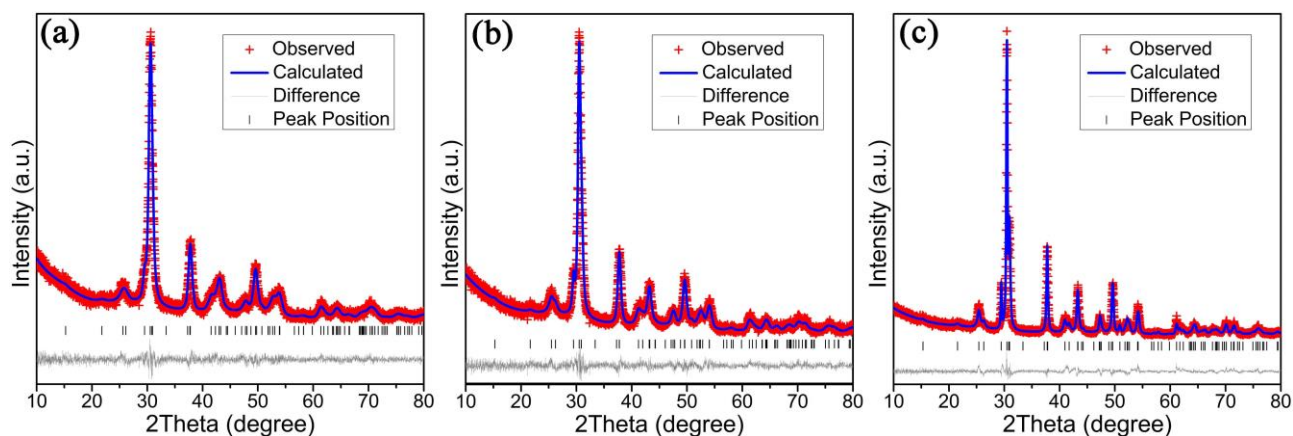

Figure S4. Profile plots from Rietveld refinement against PXD data for SnSe nanoparticles synthesised after (a) 1 min, (b) 5 min and (c) 24 h.
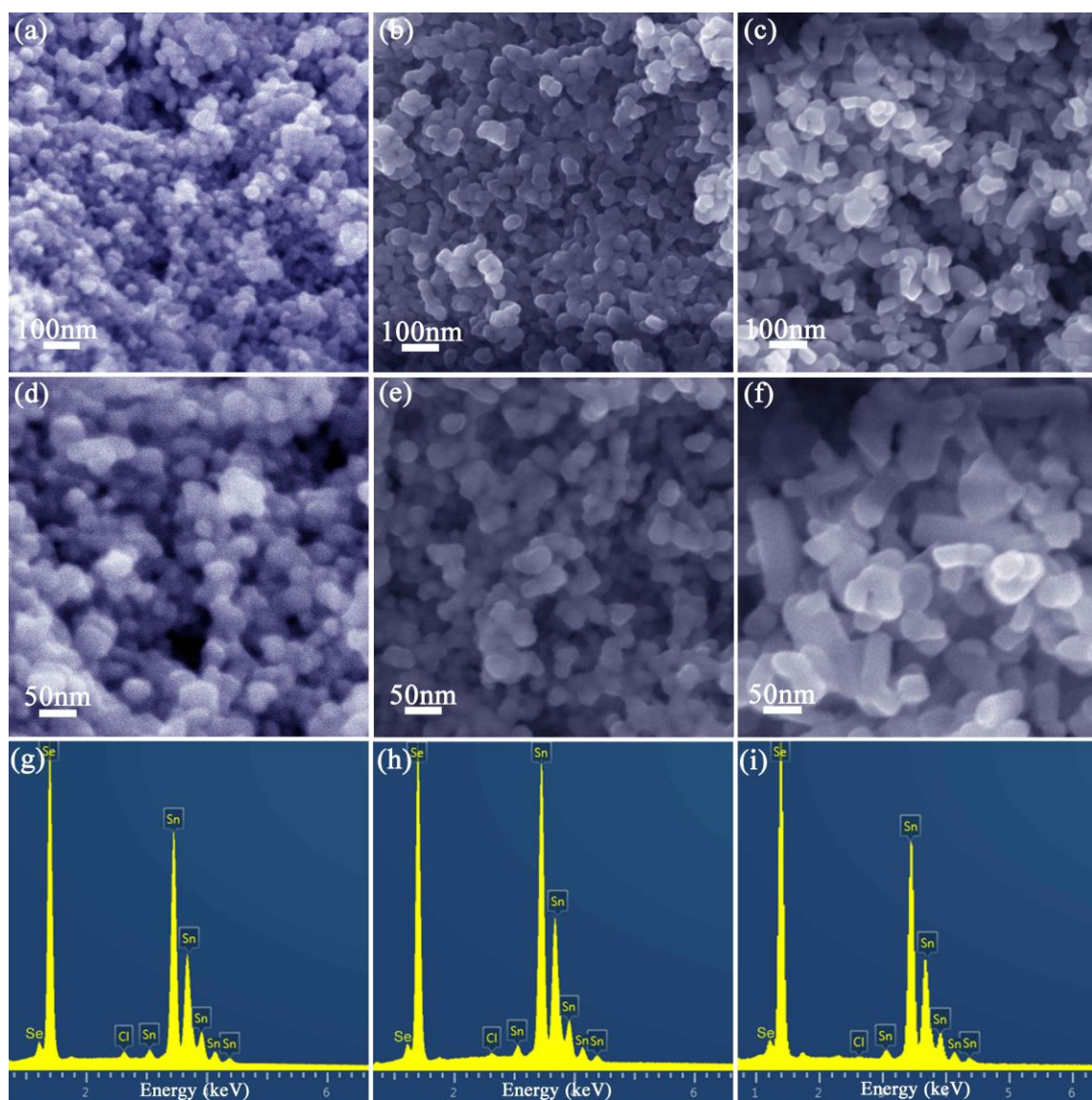
Figure S5. SEM characterisation of SnSe nanoparticles synthesised after (a,d,g) 1 min, (b,e,h) 5 min and (c,f,i) 24 h of heating: (a-f) SEM images; (g-i) EDS spectra.
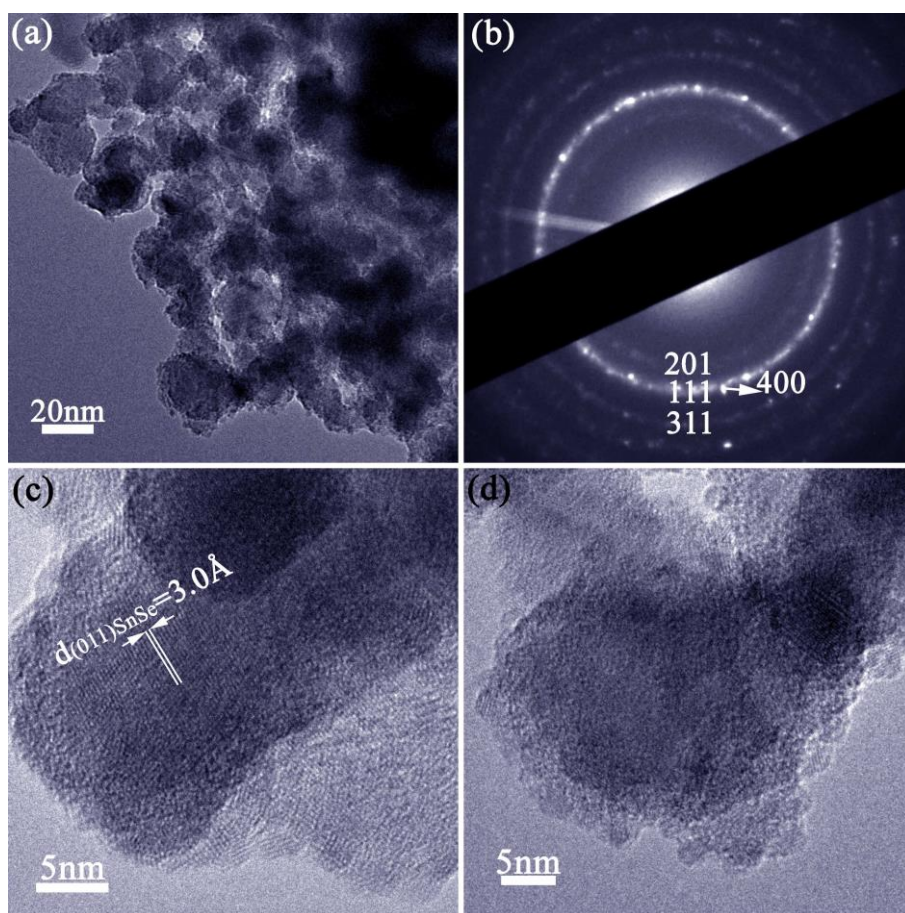
Figure S6. (a) TEM image; (b) SAED pattern and (c,d) HRTEM images of SnSe nanoparticles synthesised after 5 min of heating.
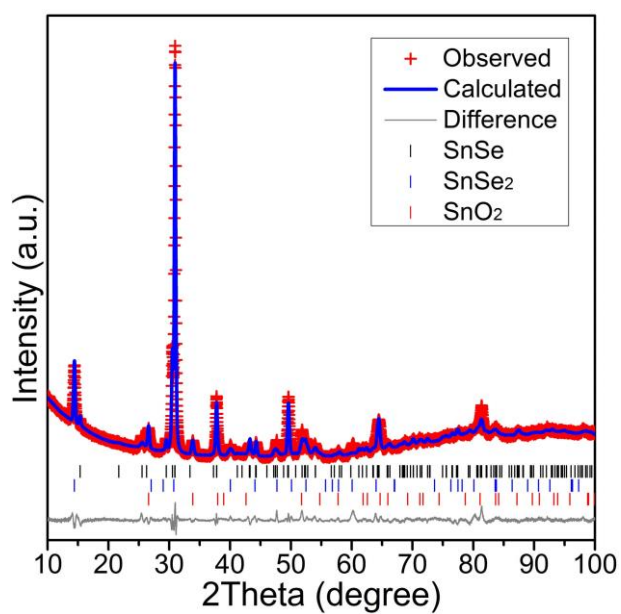

Figure S7. Profile plot from Rietveld refinement against PXD data for SnSe pellet **1**.
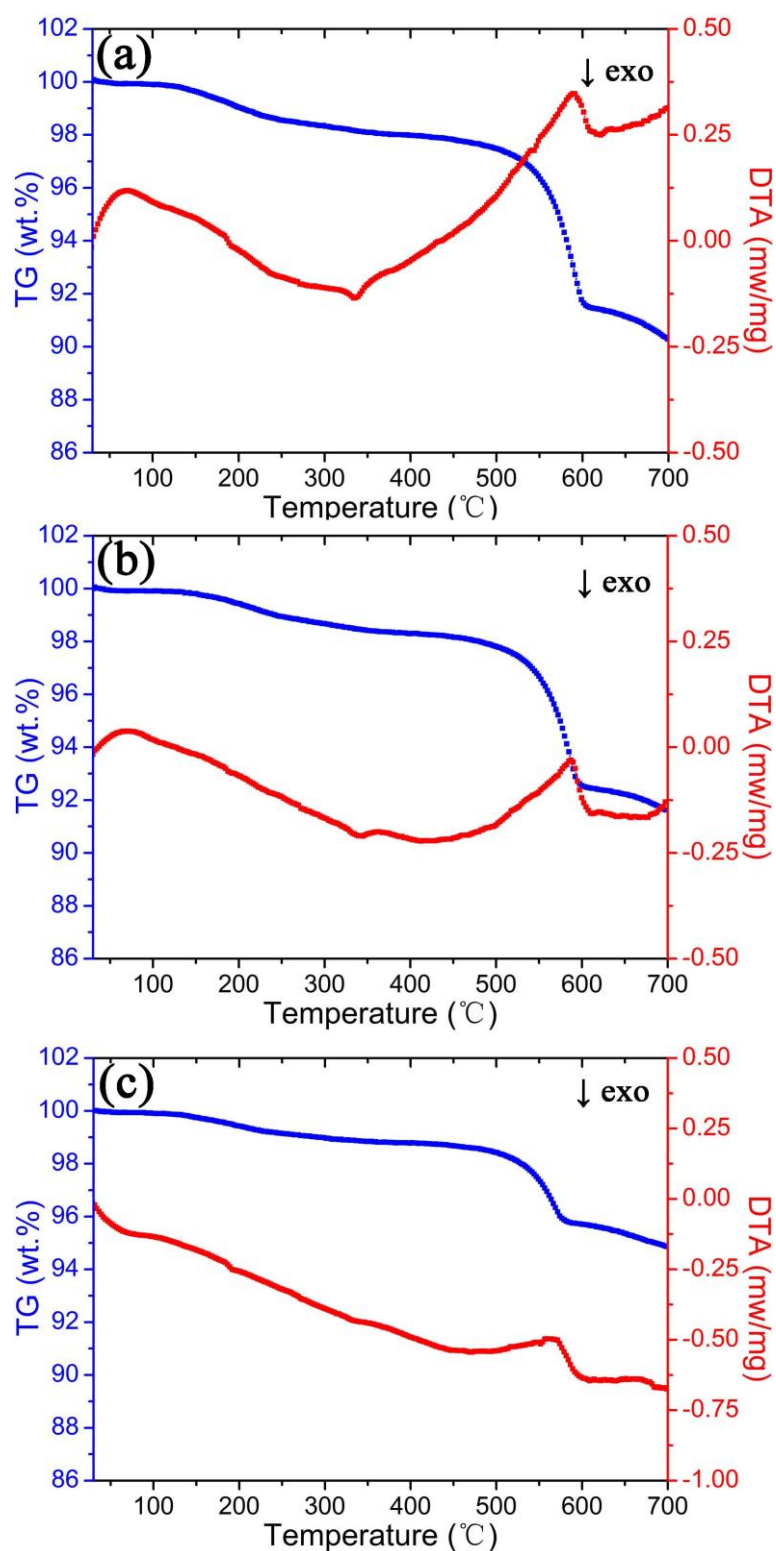
Figure S8. TG-DTA profiles of SnSe powders synthesised with different durations: (a) 1 min, (b) 2 h and (c) 24 h. The exothermic peak at ~330 ^oC and endothermic peak at ~560 ^oC correspond to the formation of SnO_2 (likely arising from the decomposition of carboxylic groups at the material surface) and volatilisation of Se, respectively.
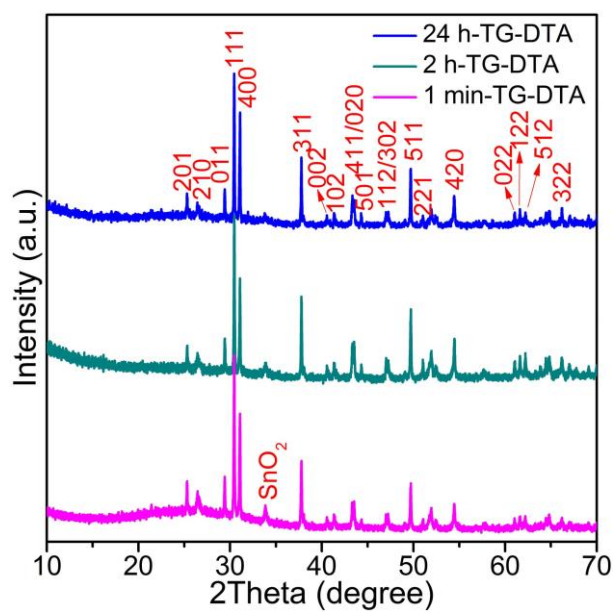
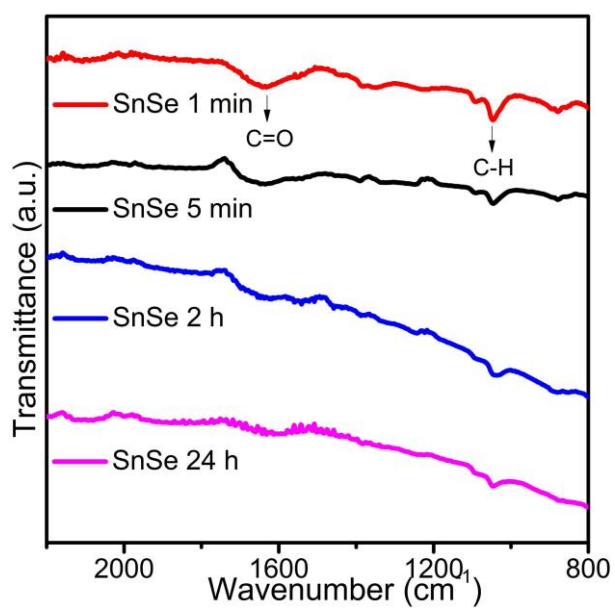**Figure S9.** PXD patterns of post-TG-DTA products from heating SnSe nanoparticles to 700 °C under an Ar flow.

Figure S10. FTIR spectra of SnSe nanoparticles synthesised with different heating durations.
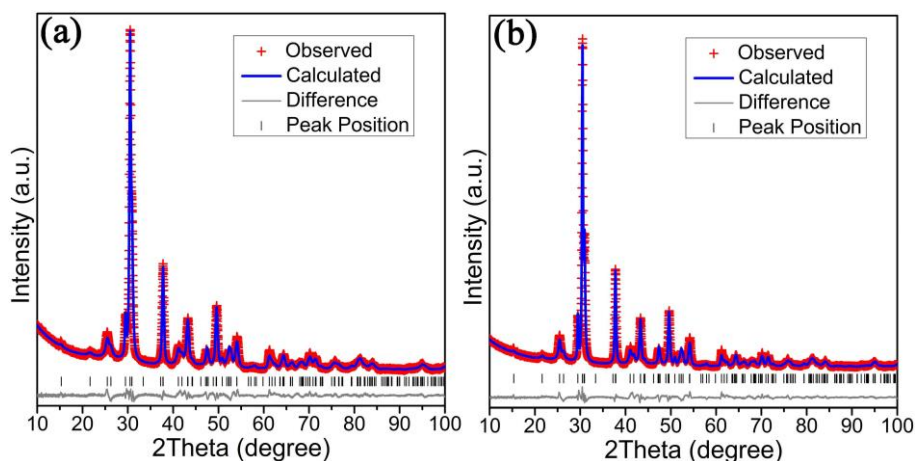
Figure S11. Profile plots from Rietveld refinement against PXD data for SnSe nanoparticles synthesised after (a) 2 h and (b) 24 h using hydrochloric acid in place of citric acid.
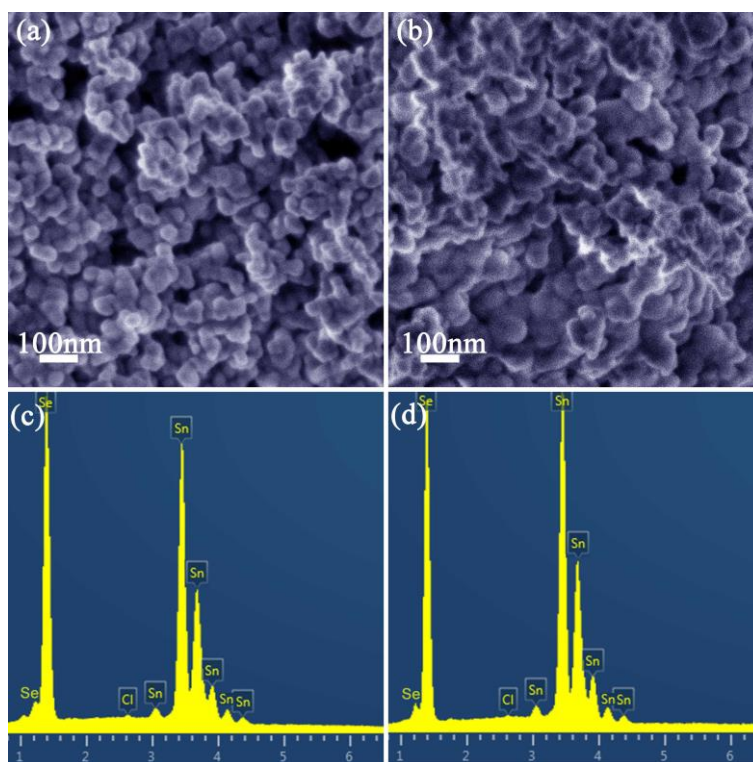
Figure S12. SEM characterisation of SnSe nanoparticles synthesised after (a,c) 2 h, (b,d) 24 h of heating using hydrochloric acid (to replace citric acid): (a,b) SEM images; (c,d) EDS spectra. The average particle sizes are 45 and 70 nm for the reaction duration of 2 and 24 h respectively, which are much larger compared to their counterparts synthesised using citric acid as the surfactant.

Figure S13. Profile plots from Rietveld refinement against PXD data for the SnSe pellets (a) **SF1** and (b) **SF2**.
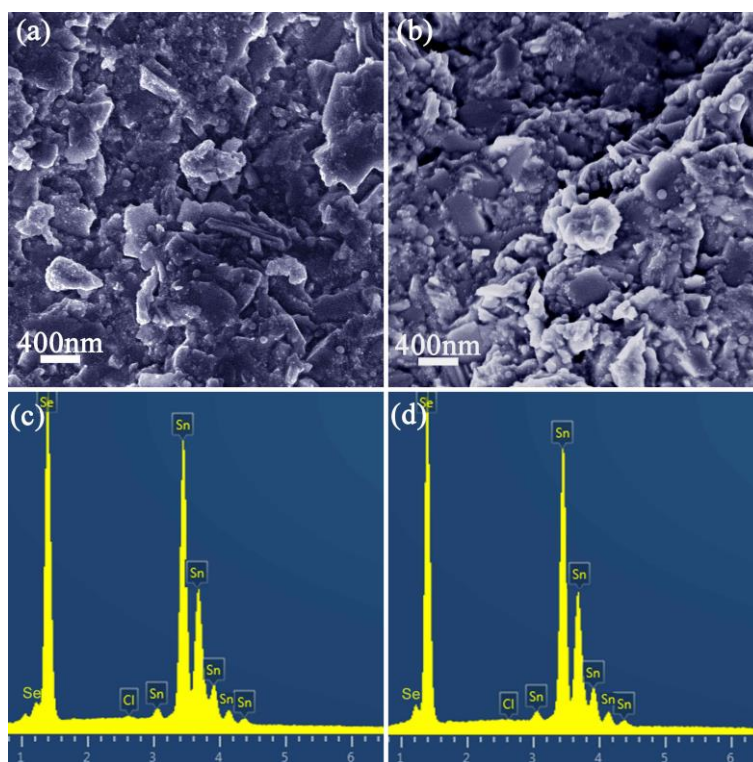
Figure S14. SEM characterisation of SnSe pellet (a,c) **SF1** and (b,d) **SF2**: (a,b) SEM images; (c,d) EDS spectra.
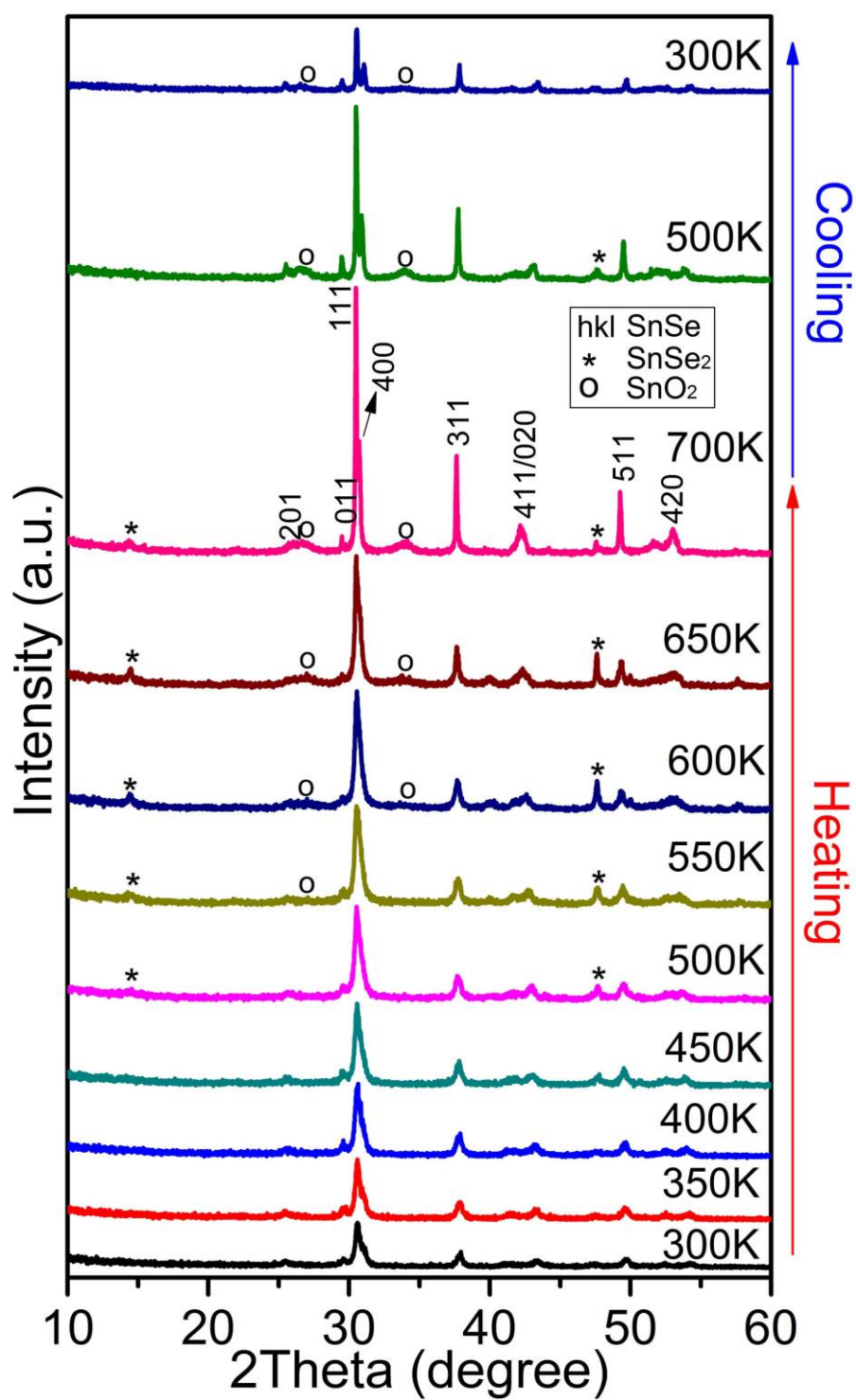
Figure S15. *In-situ* variable temperature PXD patterns of 2 h solution-synthesised SnSe nanoparticles collected at the temperatures indicated.
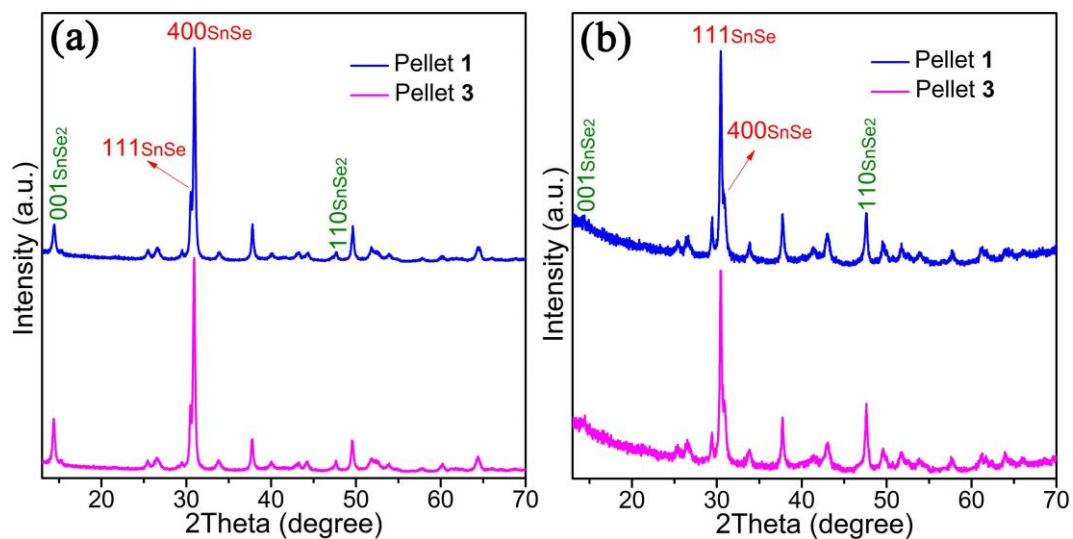
Figure S16. PXD patterns of **1** and **3** collected with the pellet faces (a) perpendicular and (b) parallel to the hot pressing direction, respectively.
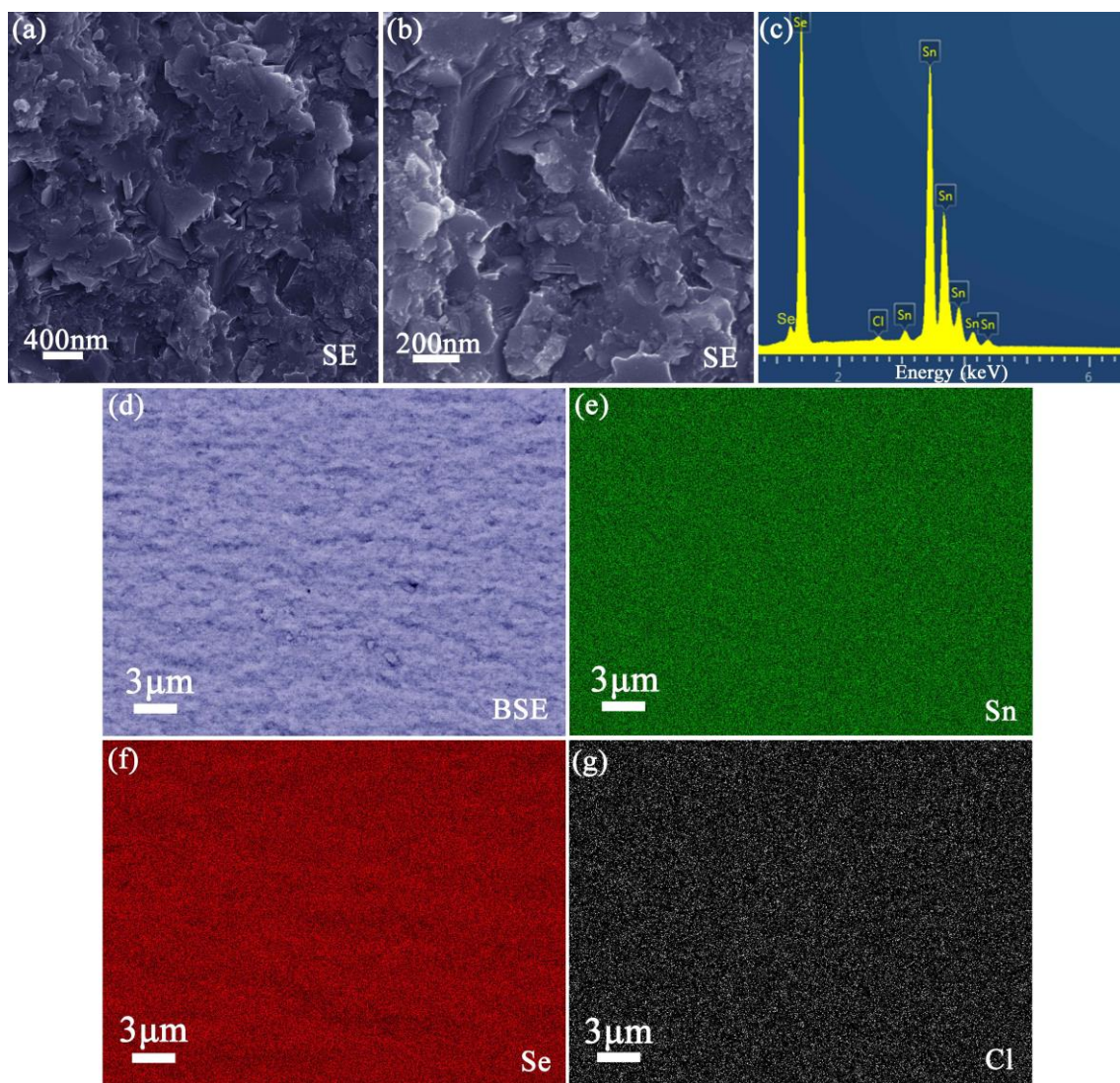
Figure S17. (a,b) Secondary electron (SE) SEM image; (c) EDS spectrum; (d) back scattered electron (BSE) SEM image and (e-g) element mapping for Sn (green), Se (red) and Cl (white) in (c), respectively for pellet **1**.
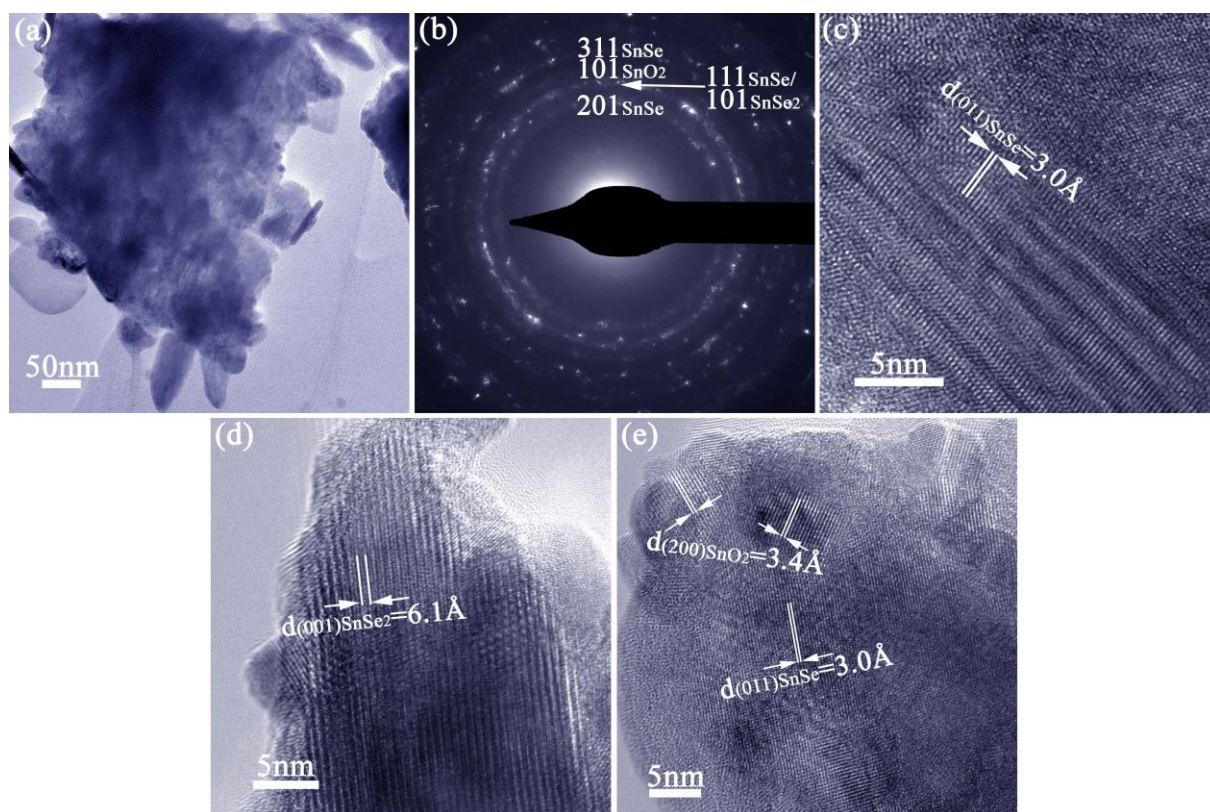
Figure S18. TEM characterisation of SnSe pellet 1: (a) typical TEM image of peeled powders; (b) SAED pattern collected from a number of plates and nanoparticles; (c) HRTEM image of an SnSe plate; (d) HRTEM image of an $SnSe_2$ plate and (e) HRTEM image a cluster of SnO_2 nanoparticles and SnSe plates. Selected d-spacings are indicated.
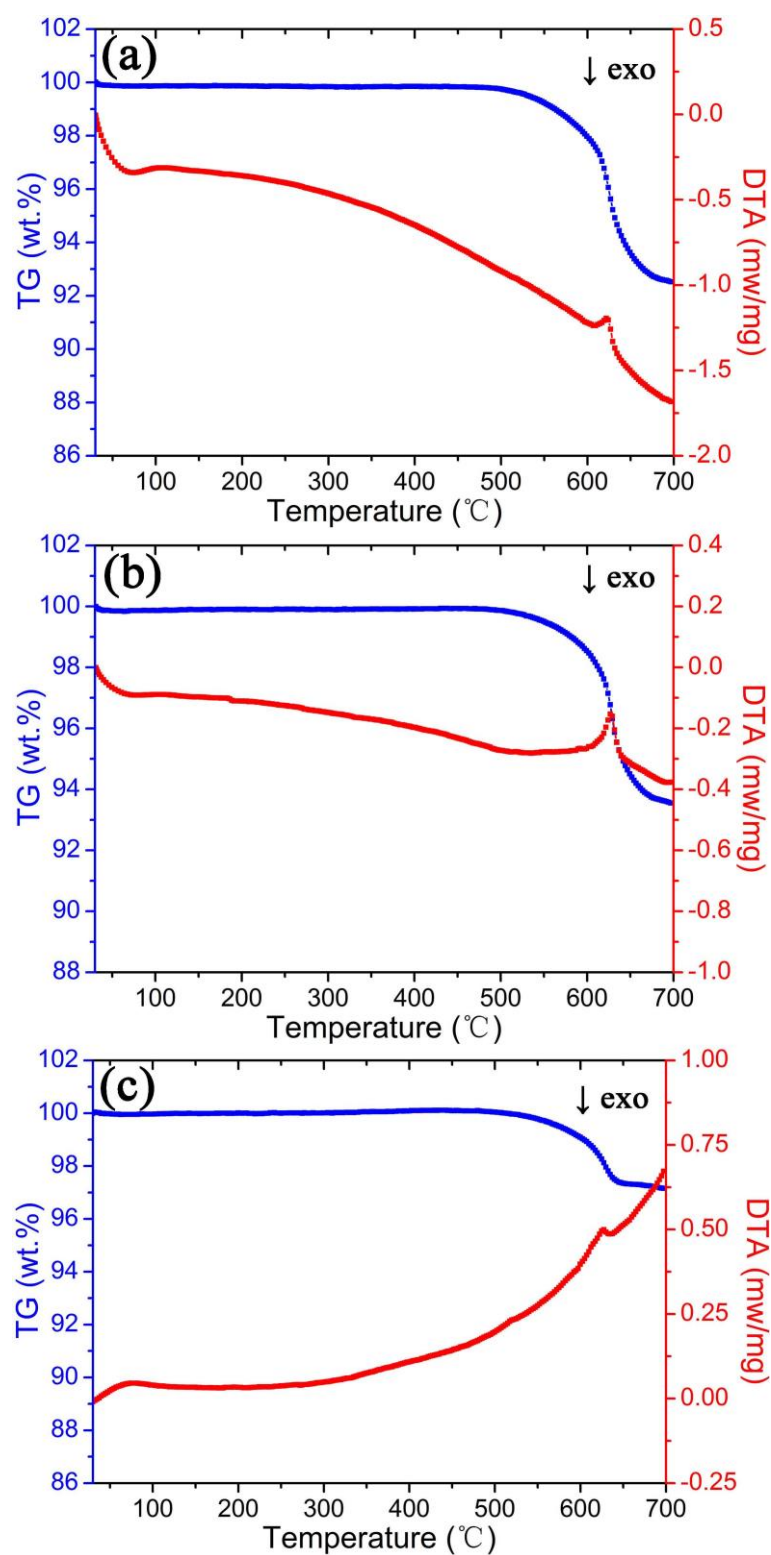
Figure S19. TG-DTA profiles of SnSe pellets: (a) **1**, (b) **3** and (c) **4**. The exothermic peak at ~630 °C corresponds to volatilisation of Se.
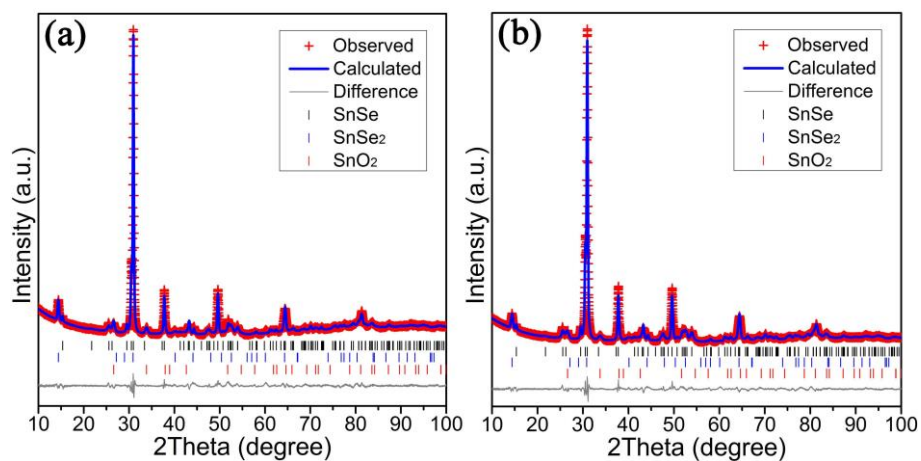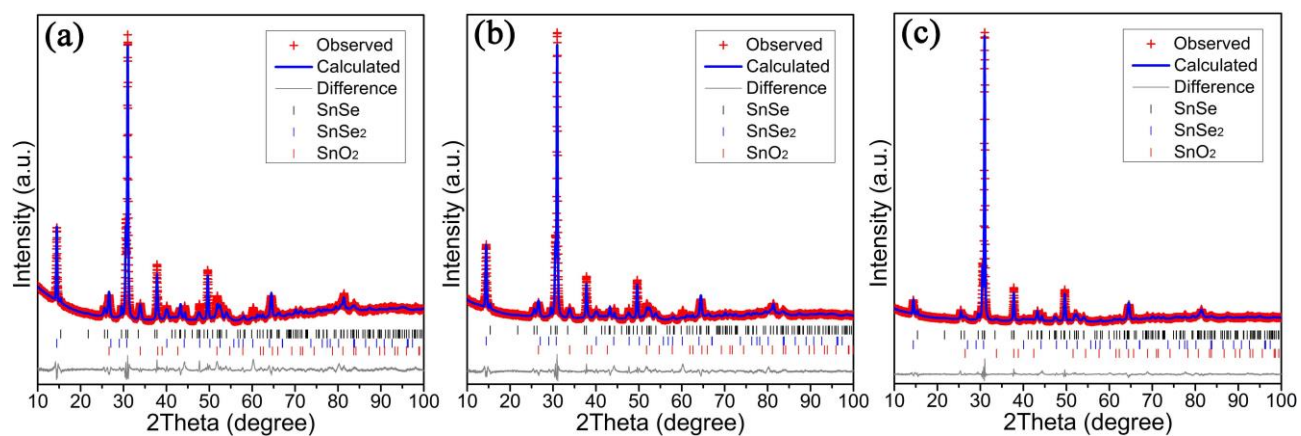
Figure S20. Profile plots from Rietveld refinement against PXD data for SnSe pellets (a) **2**, (b) **3** and (c) **4**.
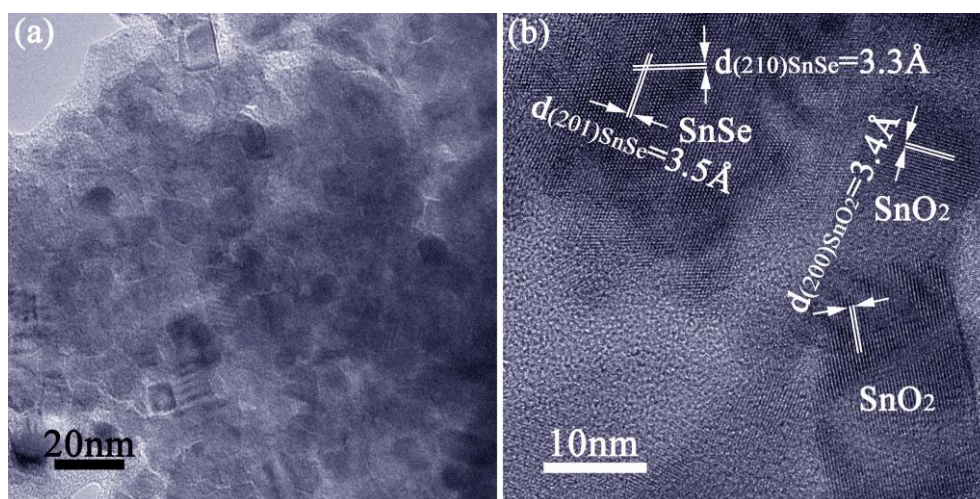
Figure S21. TEM characterisation of SnSe pellet **3**: (a) TEM image; (b) HRTEM image revealing SnO_2 nanoparticles distributed in SnSe plate.
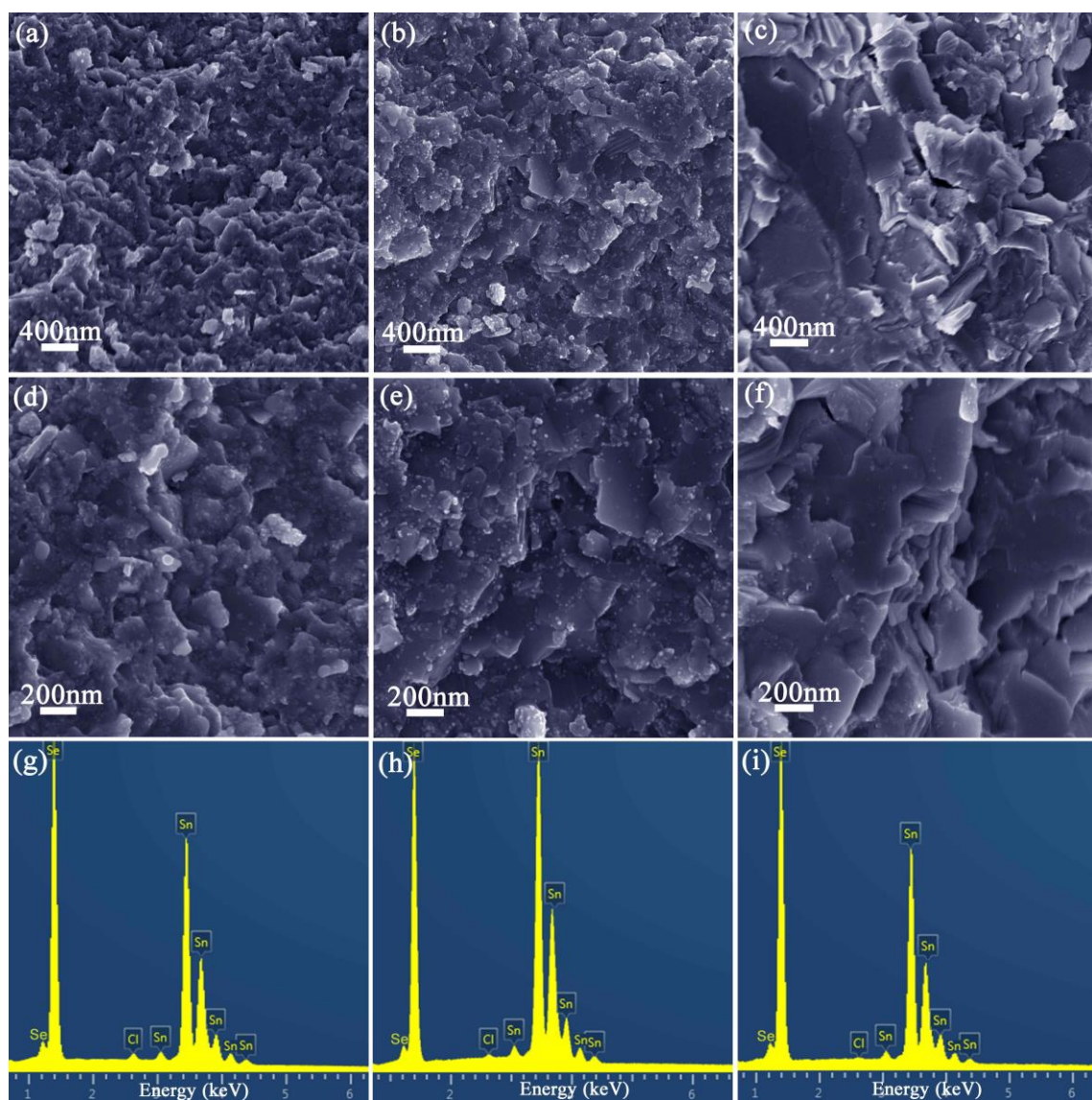
Figure S22. SEM characterisation of SnSe pellets (a,d,g) **2**, (b,e,h) **3** and (c,f,i) **4**: (a-f) SEM images; (g-i) EDS spectra.
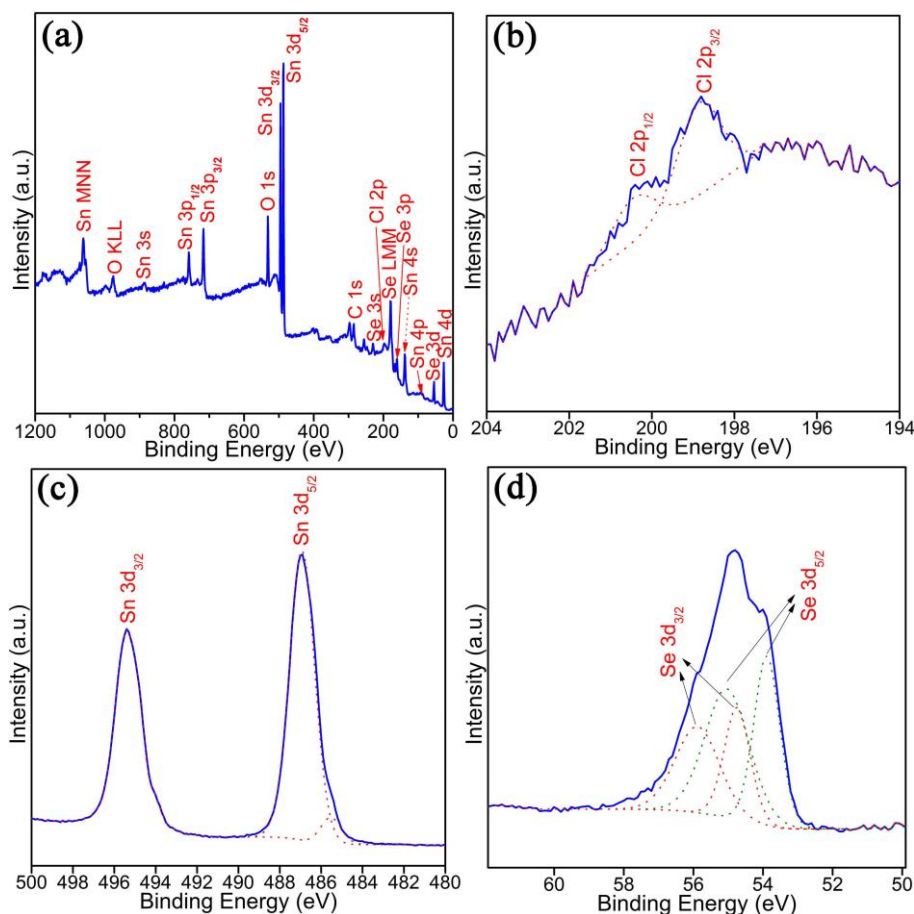
Figure S23. XPS analysis of SnSe pellet **3**: (a) survey scan; (b-d) high-resolution scan for Cl 2p, Sn 3d and Se 3d, respectively.

The high-resolution XPS spectrum of Sn (Figure S21c) shows two peak values of Sn $3d_{5/2}$: the binding energy of 486.9 eV can be rationalised in terms of Sn^{2+} bonded to Cl^{-}[8] and/or the bonding of Sn^{4+} to Se^{2-}[9] and O^{2-},[10] while the binding energy of 485.5 eV corresponds to Sn^{2+} bonded to Se^{2-}[11]. The high-resolution XPS spectrum of Se (Figure S21d) demonstrates two peak values of Se $3d_{5/2}$. The peak with a binding energy of 53.9 eV corresponds to Se^{2-} bonded to Sn^{2+}[11] and Sn^{4+}[9]. The peak at higher binding energy of 55.0 eV indicates that the surface Se^{2-} was partially oxidised. Considering that the Se $3d_{5/3}$ of Se^{0} has a binding energy of ~55.6 eV, this oxidised species could be Se_2^{2-}.[12] For the Cl 2p envelope, the area ratio of 1:2 for the two spin orbit peaks was used, an equal FWHM and a peak separation of 1.60 eV. According to quantitative XPS analysis, the Sn:Se:Cl atomic ratio is 53.3:43.5:3.2.
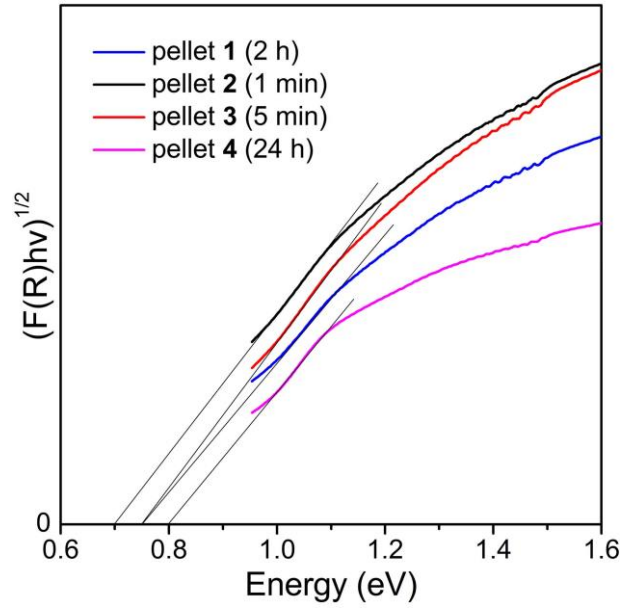
Figure S24. [F(R)hν]$^{1/2}$ *vs* energy plots from DR-UV-Vis spectroscopy data for SnSe pellets (**1-4**).

Figure S25. Repeated (runs #1-3) electrical property measurements on SnSe pellet **1** showing the variation of: (a) electrical conductivity (σ), (b) Seebeck coefficient (S) and (c) power factor ($S^2\sigma$) as a function of temperature.

Table S1 Crystallographic data for SnSe nanoparticles synthesised with different heating durations.

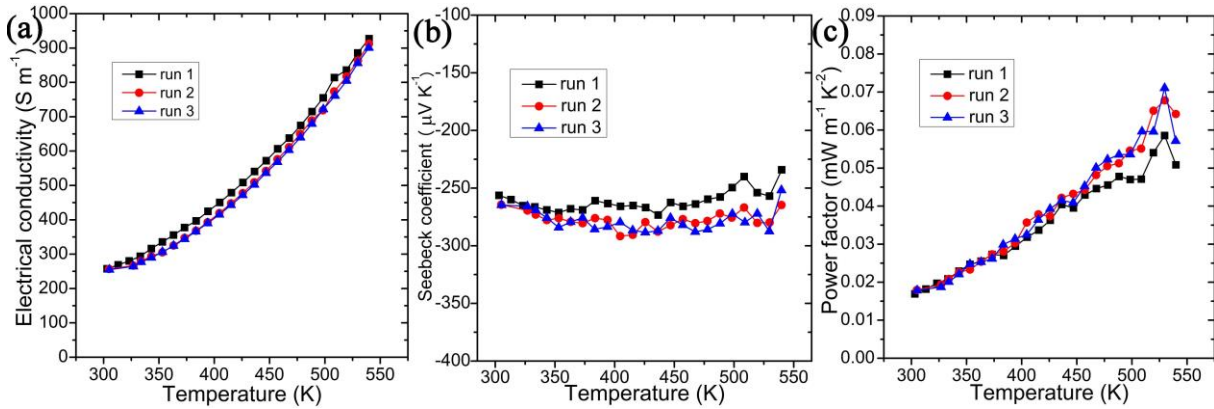| Heating duration	1 min	5 min	2 h	24 h
Chemical Formula	SnSe	SnSe	SnSe	SnSe
Crystal System	Orthorhombic	Orthorhombic	Orthorhombic	Orthorhombic
Space Group	*Pnma*	*Pnma*	*Pnma*	*Pnma*
a (Å)	11.5514(38)	11.5429(24)	11.5424(8)	11.5369(5)
b (Å)	4.1954(14)	4.1816(11)	4.1775(4)	4.1714(2)
c (Å)	4.3350(18)	4.3692(13)	4.3841(5)	4.4009(3)
Volume (Å^3)	210.08(18)	210.89(13)	211.40(4)	211.80(3)
Z	4	4	4	4
Formula Weight (g mol^{-1})	197.65	197.65	197.65	197.65
Calculated density (g cm^{-3})	6.249	6.225	6.210	6.199
R_{wp}	0.0927	0.0947	0.0692	0.0760
R_p	0.0711	0.0715	0.0500	0.0533
χ^2	1.241	1.311	4.493	8.074

Table S2 Atomic parameters for SnSe nanoparticles synthesised after 2 h heating

Atom	Wyckoff symbol	x	y	z	100*U_{iso} (Å^2)	Occupancy
Sn	4c	0.12489(19)	0.25000	0.08481(39)	5.67(8)	1
Se	4c	0.36228(27)	0.25000	0.00660(46)	3.02(8)	1

Table S3 Crystallographic data for pellet **1**

Chemical Formula	SnSe$_{0.988}$Cl$_{0.012}$	SnSe$_2$	SnO$_2$
Crystal System	Orthorhombic	Trigonal	Tetragonal
Space Group	*Pnma (62)*	*P-3m1 (164)*	*P 42/m n m (136)*
a (Å)	11.5551(8)	3.8107(19)	4.7413(8)
b (Å)	4.1968(7)		
c (Å)	4.3785(7)	6.1570(14)	3.1911(8)
Volume (Å^3)	212.33(4)	77.43(6)	71.73(3)
Z	4	1	2
Formula Weight (g mol^{-1})	197.12	276.61	150.69
Calculated density (g cm^{-3})	6.166	5.932	6.976
Phase weight percentage (wt.%)	79.15(11)	11.06(25)	9.79(16)
R_{wp}	0.0703		
R_p	0.0468		
χ^2	8.088		

Table S4 Crystallographic data for SnSe nanoparticles synthesised using hydrochloric acid (replacing citric acid and heating for 2 and 24 h respectively)

Reaction duration	2 h	24 h
Chemical Formula	SnSe	SnSe
Crystal System	Orthorhombic	Orthorhombic
Space Group	*Pnma*	*Pnma*
a (Å)	11.5476(7)	11.5404(6)
b (Å)	4.1817(4)	4.1743(3)
c (Å)	4.3770(4)	4.3926(4)
Volume (Å^3)	211.36(4)	211.61(3)
Z	4	4
Formula Weight (g mol^{-1})	197.65	197.65
Calculated density (g cm^{-3})	6.211	6.204
R_{wp}	0.0643	0.0783
R_p	0.0464	0.0554
χ^2	5.570	8.697

Table S5 Crystallographic data for pellet **SF1**

Chemical Formula	$SnSe_{0.994}Cl_{0.006}$	$SnSe_2$	SnO_2
Crystal System	Orthorhombic	Trigonal	Tetragonal
Space Group	*Pnma (62)*	*P-3m1 (164)*	*P 42/m n m (136)*
a (Å)	11.5576(7)	3.7885(36)	4.7402(11)
b (Å)	4.2013(5)		
c (Å)	4.3710(6)	6.1601(18)	3.1931(12)
Volume (Å^3)	212.24(3)	76.57(11)	71.75(4)
Z	4	1	2
Formula Weight (g mol^{-1})	197.65	276.61	150.69
Calculated density (g cm^{-3})	6.185	5.998	6.975
Phase weight percentage (wt.%)	85.40(6)	6.66(23)	7.94(14)
R_{wp}	0.0766		
R_p	0.0548		
χ^2	6.991		

Table **S6** Crystallographic data for pellet **SF2**

Chemical Formula	SnSe$_{0.998}$Cl$_{0.002}$	SnSe$_2$	SnO$_2$
Crystal System	Orthorhombic	Trigonal	Tetragonal
Space Group	*Pnma (62)*	*P-3m1 (164)*	*P 42/m n m (136)*
a (Å)	11.5574(6)	3.7957(34)	4.7430(18)
b (Å)	4.2023(4)		
c (Å)	4.3677(4)	6.1579(24)	3.2019(21)
Volume (Å^3)	212.13(3)	76.83(11)	72.03(6)
Z	4	1	2
Formula Weight (g mol^{-1})	197.56	276.61	150.69
Calculated density (g cm^{-3})	6.186	5.978	6.948
Phase weight percentage (wt.%)	87.71(5)	6.84(23)	5.46(14)
R$_{wp}$	0.0789		
R$_p$	0.0582		
χ^2	7.369		

Table S7 Crystallographic data for pellet **2**

Chemical Formula	SnSe$_{0.975}$Cl$_{0.025}$	SnSe$_2$	SnO$_2$
Crystal System	Orthorhombic	Trigonal	Tetragonal
Space Group	*Pnma (62)*	*P-3m1 (164)*	*P 42/m n m (136)*
a (Å)	11.5579(9)	3.8107(15)	4.7413(9)
b (Å)	4.1991(7)		
c (Å)	4.3749(7)	6.1573(13)	3.1904(9)
Volume (Å^3)	212.33(4)	77.43(5)	71.72(3)
Z	4	1	2
Formula Weight (g mol^{-1})	196.56	276.61	150.69
Calculated density (g cm^{-3})	6.149	5.932	6.978
Phase weight percentage (wt.%)	71.57(15)	14.62(25)	13.81(18)
R$_{wp}$	0.0944		
R$_p$	0.0665		
χ^2	11.66		

Table S8 Crystallographic data for pellet **3**

Chemical Formula	SnSe$_{0.985}$Cl$_{0.015}$	SnSe$_2$	SnO$_2$
Crystal System	Orthorhombic	Trigonal	Tetragonal
Space Group	*Pnma (62)*	*P-3m1 (164)*	*P 42/m n m (136)*
a (Å)	11.5583(8)	3.8110(17)	4.7412(10)
b (Å)	4.2026(7)		
c (Å)	4.3691(6)	6.1559(1)	3.1903(11)
Volume (Å^3)	212.23(4)	77.43(6)	71.71(4)
Z	4	1	2
Formula Weight (g mol^{-1})	197.02	276.61	150.69
Calculated density (g cm^{-3})	6.166	5.932	6.978
Phase weight percentage (wt.%)	71.73(14)	15.28(25)	13.00(18)
R$_{wp}$	0.0984		
R$_p$	0.0677		
χ^2	7.648		

Table S9 Crystallographic data for pellet **4**

Chemical Formula	$SnSe_{0.994}Cl_{0.006}$	$SnSe_2$	SnO_2
Crystal System	Orthorhombic	Trigonal	Tetragonal
Space Group	*Pnma (62)*	*P-3m1 (164)*	*P 42/m n m (136)*
a (Å)	11.5421(5)	3.8119(34)	4.7635(30)
b (Å)	4.1909(4)		
c (Å)	4.3861(4)	6.1534(16)	3.1968(34)
Volume ($Å^3$)	212.16(3)	77.43(11)	72.54(10)
Z	4	1	2
Formula Weight (g mol^{-1})	197.38	276.61	150.69
Calculated density (g cm^{-3})	6.179	5.932	6.899
Phase weight percentage (wt.%)	90.41(4)	6.08(21)	3.51(16)
R_{wp}	0.0867		
R_p	0.0620		
χ^2	5.880		

References:

[1]   a) A. C. Larson, R. B. Von Dreele, General Structure Analysis System (GSAS); Los Alamos National Laboratory Report LAUR 86-748; Los Alamos National Laboratory, 1994; b) B. H. Toby, *J. Appl. Crystallogr.* 2001, *34*, 210-213.

[2]   A. S. Avilov, R. M. Imamov, S. N. Navasardyan, *Kristallografiya* 1979, *24*, 874-875.

[3]   F. A. S. Al-Alamy, A. A. Balchin, M. White, *J. Mater. Sci.* 1977, *12*, 2037-2042.

[4]   W. H. Baur, A. A. Khan, *Acta Crystallogr. Sect. B* 1971, *27*, 2133-2139.

[5]   M. Ibáñez, R. J. Korkosz, Z. S. Luo, P. Riba, D. Cadavid, S. Ortega, A. Cabot, M. G. Kanatzidis, *J. Am. Chem. Soc.* 2015, *137*, 4046-4049.

[6]   Y.-X. Chen, Z.-H. Ge, M. Yin, D. Feng, X.-Q. Huang, W. Zhao, J. He, *Adv. Funct. Mater.* 2016, DOI: 10.1002/adfm.201602652.

[7]   a) S. W. Finefrock, G. Zhang, J.-H. Bahk, H. Fang, H. Yang, A. Shakouri, Y. Wu, *Nano Lett.* 2014, *14*, 3466-3473; b) C. Kim, D. H. Kim, H. Kim, J. S. Chung, *ACS Appl. Mater. Interfaces* 2012, *4*, 2949-2954; c) H. F. He, X. F. Li, Z. Q. Chen, Y. Zheng, D. W. Yang, X. F. Tang, *J. Phys. Chem. C* 2014, *118*, 22389-22394.

[8]   H. Willemen, D. F. Van De Vondel, G. P. Van Der Kelen, *Inorg. Chim. Acta* 1979, *34*, 175-180.

[9]   C. H. de Groot, C. Gurnani, A. L. Hector, R. M. Huang, M. Jura, W. Levason, G. Reid, *Chem. Mater.* 2012, *24*, 4442-4449.

[10]   W. K. Choi, H. J. Jung, S. K. Koh, *J. Vac. Sci. Technol. A* 1996, *14*, 359-366.

[11]   M. A. Franzman, C. W. Schlenker, M. E. Thompson, R. L. Brutchey, *J. Am. Chem. Soc.* 2010, *132*, 4060-4061.

[12]   X. M. Zhou, P. Gao, S. C. Sun, D. Bao, Y. Wang, X. B. Li, T. T. Wu, Y. J. Chen, P. P. Yang, *Chem. Mater.* 2015, *27*, 6730-6736.